J|A|C|S
ARTICLES
Published on Web 03/27/2004

Anisotropic Small Amplitude Peptide Plane Dynamics in Proteins from Residual Dipolar Couplings

Pau Bernadó and Martin Blackledge*

Contribution from the Institut de Biologie Structurale Jean-Pierre Ebel, UJF−CNRS−CEA, 41 rue Jules Horowitz, 38027 Grenoble Cedex, France

Received June 30, 2003; E-mail: Martin.Blackledge@ibs.fr

Abstract: The effect of small amplitude anisotropic peptide plane motion on residual dipolar couplings (RDC) measured in proteins has been investigated. RDC averaging effects in the presence of GAF (Gaussian axial fluctuation) motions are found to vary strongly depending on the peptide plane orientation. Even low amplitude dynamics can significantly affect derived alignment tensor parameters if this motion is not taken into account. An analytical description of averaged $N-^{N}H$ RDCs is introduced that includes basic GAF-like motion. The averaging depends on the orientation of the peptide plane (α, β, γ) in the alignment frame and on the motional amplitude (σ). This expression is used to investigate the presence of anisotropic reorientational dynamics in proteins by incorporating σ as an additional parameter into the alignment tensor analysis. Average GAF amplitudes (σ_{av}) are determined for secondary structural elements from single experimental $N-^{N}H$ RDC data sets from five different proteins, in combination with high-resolution structural models. This yields statistically significant improvement over the static description, and detects σ_{av} values ranging from 14.4 to 17.0° for the different proteins. A higher value of $\sigma_{av} = 20°$ from loop regions was found using two independent sets of $N-^{N}H$ RDC in the protein lysozyme, for which a very high-resolution structure is available. Comparison of fitting behavior over 13 structures from lysozyme of crystal diffraction resolution ranging from 0.9 to 2.1Å indicates a small spread of motional amplitudes, demonstrating that the method is robust up to this level of resolution. A combined definition of $^{\alpha}C-C'$ and $N-^{N}H$ RDC under the influence of GAF motions allows simultaneous fitting of both RDC. Application to three proteins leads to similar σ_{av} values and a more significant improvement with respect to the static model. Using the GAF model to describe conformationally averaged RDC is important for two reasons: a more accurate definition of the alignment tensor magnitude can be derived, and the method can be used to detect average small amplitude motions in protein backbones from readily accessible data, on time scales not easily sampled by other NMR techniques.

Introduction

Dipolar couplings measured under conditions of weak alignment[1,2] provide highly precise information defining the orientation of internuclear bonds relative to a molecule-fixed frame, a characteristic that makes these parameters particularly powerful for biomolecular structure determination.[3−5] Although static models can closely reproduce experimentally measured residual dipolar couplings (RDCs), these measurements actually report on averages over relatively long time scales as well as over the entire population ensemble. It is of great interest to access this information, as the time scale that is sampled, up to the millisecond range, is highly complementary to dynamics in the picosecond to nanosecond time scale detected from NMR spin relaxation studies.[6] The importance of this conformational averaging has been recognized since the earliest work on weak alignment of proteins.[7,8] Most commonly RDCs have been used to invoke differential dynamics when alignment characteristics change significantly in distinct regions of a molecule, for example in multidomain proteins[9] or between sugar moieties in carbohydrates.[10] A similar approach has been used to study the local dynamics of dipeptide fragments containing up to eight different spin-pair couplings along the protein backbone.[11]

The effect of simple motional averaging of an axially symmetric nature on measured RDC can be expressed as an order parameter, S, and therefore a phenomenon that linearly scales expected RDC values for the static vector. Assuming that no additional motion occurs, this parameter can be directly related to the S^2 order parameter encountered in ^{15}N relaxation

(1) Tjandra, N.; Bax, A. *Science* **1997**, *278*, 1111−1114.
(2) Tolman, J. R.; Flanagan, J. M.; Kennedy, M. A.; Prestegard, J. H. *Proc. Natl. Acad. Sci.* **1995**, *92*, 9279−9283.
(3) Prestegard, J. H.; Al-Hashimi, H. M.; Tolman, J. R. *Q. Rev. Biophys.* **2000**, *33*, 371−424.
(4) Bax, A.; Kontaxis, G.; Tjandra, N. *Methods Enzymol.* **2001**, *339*, 127−174.
(5) de Alba, E.; Tjandra, N. *Prog. Nucl. Magn. Reson. Spectrosc.* **2002**, *40*, 175−197.
(6) Tolman, J. R. *Curr. Opin. Struct. Biol.* **2001**, *11*, 532−539.
(7) Tolman, J. R.; Flanagan, J. M.; Kennedy, M. A.; Prestegard, J. H. *Nat. Struct. Biol.* **1997**, *4*, 292−297.
(8) Bax, A.; Tjandra, N. *Nat. Struct. Biol.* **1997**, *4*, 254−256.
(9) Fischer, M. W. F.; Losonczi, J. A.; Weaver, J. L.; Prestegard, J. H. *Biochemistry* **1999**, *38*, 9013−9022.
(10) Tian, F. F.; Al-Hashimi, H. M.; Craighead, J. L.; Prestegard, J. H. *J. Am. Chem. Soc.* **2001**, *123*, 485−492.
(11) Tolman, J. R.; Al-Hashimi, H. M.; Kay L. E.; Prestegard, J. H. *J. Am. Chem. Soc.* **2001**, *123*, 1416−1424.

studies of proteins.[12,13] Recently, the possibility of studying more complex motional properties of individual N−^{N}H vectors has been elegantly demonstrated.[14] In this work, analysis of a 10-ns MD simulation showed that complex dynamic averaging effects could be detected if at least five independent sets of RDCs were available. This methodology is essentially "model-free" as no specific motional model is invoked in the definition. The direction and amplitude of angular sampling of the internuclear vector is described purely in terms of average second-order spherical harmonics $\langle Y_{2M} \rangle$. The application of this methodology to RDCs measured in 11 different alignment media subsequently allowed the authors to characterize the motional properties of N−^{N}H vectors along the peptide chain of ubiquitin.[15] This study detects a degree of mobility that is not visible from relaxation studies, presumably therefore in the nano to millisecond time scale. A philosophically similar model-free analysis has recently been published, which describes the averaged RDCs, again from multiple alignment media, in terms of a single matrix. This approach determines the elements of unknown matrices containing both structural and dynamic information and the alignment properties of the media that in combination can give rise to these data.[16] In this case, the authors do not present absolute motional amplitudes, but show relative order-parameters that show some correlation with those derived from ^{15}N relaxation.[17]

A more recent investigation has demonstrated the use of multiple RDCs from different spin-pairs in the peptide unit measured in up to five alignment media to study the fine details of backbone structure and dynamics in solution.[18] This study demonstrates that even a high-resolution crystal structure can be further refined using C′−C$^{\alpha}$ and C′−N RDCs to produce a single backbone conformation in agreement with all five sets of N−^{N}H couplings. This provides evidence for somewhat smaller amplitude N−^{N}H vector motions than those identified by the model-free analyses described above.

Importantly all of these analyses identify the possible presence of anisotropic components to the N−^{N}H vector motion. It is accepted that backbone dynamics are complex processes and that no single geometric model will be universal. Nevertheless, extensive molecular simulations in peptides[19] and in ubiquitin[20] have shown that anisotropic motions, in the form of Gaussian axial fluctuations (GAF) around the average position, can be useful to characterize fundamental backbone motions in proteins. Brüschweiler and collaborators have shown that rigid peptide plane fragment motion can be described by a three-dimensional GAF motion (3D-GAF) comprising independent rotations of amplitude $\sigma_{\alpha,\beta,\gamma}$ around three orthogonal axes (α, β, γ) fixed in the peptide plane. The main axis of rotation, γ, lies long the axis C$^{\alpha}_{i-1}$−C$^{\alpha}_{i}$, and a reduction of the 3D-GAF model comprising this major component alone (1D-GAF) was initially proposed to interpret spin relaxation derived order parameters.[21] The other two axis, α and β, lie in the peptide plane and perpendicular to it, respectively. ^{15}N and ^{13}C relaxation rates have been fitted to this, or similar dynamic models.[19,20,22,23] For the case of ubiquitin, angular amplitudes of $\sigma_{\gamma} = 16.6°$ and $\sigma_{\alpha} = \sigma_{\beta} = 6.7°$ were derived for those residues displaying a Gaussian axial fluctuation behavior in the MD simulation.[20] Ulmer et al. also note that their analysis of N−^{N}H RDCs measured in five alignment media can be in agreement with the presence of anisotropic motion in protein G.[18] The RDC averaging observed in this study allows the authors to place a limit on the amplitude of anisotropic motions that is similar to that derived from spin relaxation analysis.

Following these leads, we investigate here the effects of anisotropic peptide plane motions on RDCs and assess the possibility of incorporating this kind of dynamic motion into the analysis of experimental data. To achieve this, we have used the 1D- and 3D-GAF geometric models to describe local peptide chain motions. From numerical simulations, we observe highly heterogeneous averaging effects, depending on the orientation of the peptide plane with respect to the alignment tensor. We initially demonstrate some salient features of RDC averaging in this motional regime and the expected effects of this averaging on alignment tensor determination. These effects are reproduced in experimental data sets from our laboratory and in other published data sets and are found to perturb the precision to which molecular alignment tensors can be determined. This is important because imprecision in alignment tensor determination will affect the eventual accuracy to which both structure and dynamics of proteins can be extracted from experimental RDC. An analytical expression is then presented that describes the dependence of the averaged RDC on peptide plane orientation and motional amplitude σ under the influence of GAF motions. This allows the incorporation of an average amplitude for peptide plane reorientation into the analysis of single-medium N−^{N}H RDC data sets or combined N−^{N}H and $^{\alpha}$C$_{i-1}$−$^{\alpha}$C$_{i}$ data sets. We present the application of this approach to the study of anisotropic peptide plane dynamics in six different proteins, detecting average σ values of around 15° in secondary structural elements. This analysis provides a statistically significant improvement compared to static, or axially symmetric descriptions. All of this work demonstrates the utility of using the GAF motional model for the interpretation of dynamically averaged RDC measured in proteins. This general method allows the estimation of average amplitudes of anisotropic motions and provides a more precise determination of alignment tensor magnitude from experimental data.

Theory

Analytical Description of RDCs under 1D- and 3D-GAF Motional Averaging. In the presence of directional averaging the measured residual dipolar coupling is given by

$$\langle D_{ij} \rangle = K_0 \left[A_a \langle 3\cos^2\theta - 1 \rangle + \frac{3}{2} A_r \langle \sin^2\theta \cos 2\phi \rangle \right] \quad (1)$$

where

$$K_0 = -\frac{\gamma_i \gamma_j \mu_0 h}{16\pi r^3}$$

(12) Lipari, G.; Szabo, A. *J. Am. Chem. Soc.* **1982**, *104*, 4546−4559.
(13) Lipari, G.; Szabo, A. *J. Am. Chem. Soc.* **1982**, *104*, 4559−4570.
(14) Meiler, J.; Prompers, J. J.; Peti, W.; Griesinger, C.; Brüschweiler, R. *J. Am. Chem. Soc.* **2001**, *123*, 6098−6107.
(15) Peti, W.; Meiler, J.; Brüschweiler, R.; Griesinger, C. *J. Am. Chem. Soc.* **2002**, *124*, 5822−5833.
(16) Tolman, J. R. *J. Am. Chem. Soc.* **2002**, *124*, 12020−12030.
(17) Briggman, K. B.; Tolman, J. R. *J. Am. Chem. Soc.* **2003**, *125*, 10164−10165.
(18) Ulmer, T. S.; Ramirez, B. E.; Delaglio, F.; Bax, A. *J. Am. Chem. Soc.* **2003**, *125*, 9179−9191.
(19) Bremi, T.; Brüschweiler, R. *J. Am. Chem. Soc.* **1997**, *119*, 6672−6673.
(20) Lienin, S. F.; Bremi, T.; Brutscher, B.; Brüschweiler, R.; Ernst, R. R. *J. Am. Chem. Soc.* **1998**, *120*, 9870−9879.
(21) Brüschweiler, R.; Wright, P. E. *J. Am. Chem. Soc.* **1994**, *116*, 8426−8427.

where angular parentheses indicate the average angular terms. A_a and A_r are the axial and rhombic components of the alignment tensor, and θ and ϕ describe the orientation of the *ij* vector relative to the alignment tensor. We can also express this in terms of averaged spherical harmonics:

$$\langle D_{ij}\rangle = KA_a\sqrt{\frac{16\pi}{5}}\left\{\langle Y_{20}(\theta,\phi)\rangle + \sqrt{\frac{3}{8}}R(\langle Y_{22}(\theta,\phi)\rangle + \langle Y_{2-2}(\theta,\phi)\rangle)\right\} \quad (2)$$

where $R = (A_r/A_a)$. The advantage of this description is that we can easily transform eq 2 from one reference frame to another using the transformation properties of the average spherical harmonics rotated by Euler angles (α, β, γ):

$$R(\alpha,\beta,\gamma)\, Y_{2,M}(\theta,\phi) = \sum_{M'=-2}^{+2} e^{-i\alpha M'}\, d_{M'M}^{(2)}(\beta) e^{-i\gamma M} Y_{2,M'}(\theta,\phi) \quad (3)$$

Following the logic presented previously,[3,14,15] we then describe simple motional averaging of the spherical harmonics in the peptide plane frame, and transform these into the alignment tensor frame using the appropriate Euler rotation for each individual peptide plane:

$$\langle D_{ij}\rangle = KA_a\sqrt{\frac{16\pi}{5}}\left\{\sum_{M'=-2}^{+2} e^{-i\alpha_{pp}M'} d_{M'0}^{(2)}(\beta_{pp})\langle Y_{2M'}(\theta,\phi)\rangle + \sqrt{\frac{3}{8}}R\Big(\sum_{M'=-2}^{+2} e^{-i\alpha_{pp}M'} d_{M'2}^{(2)}(\beta_{pp}) e^{-i\gamma_{pp}M}\langle Y_{2M'}(\theta,\phi)\rangle + \sum_{M'=-2}^{+2} e^{-i\alpha_{pp}M'} d_{M'2}^{(2)}(\beta_{pp}) e^{-i\gamma_{pp}M}\langle Y_{2M'}(\theta,\phi)\rangle\Big)\right\} \quad (4)$$

In this case the rotation (α_{pp}, β_{pp}, γ_{pp}) describes the transformation from the alignment tensor principal axis system into the local peptide plane frame. In this local frame the *z*-axis lies along the average NH direction, and the local *y*-axis along the projection of the average $^{\alpha}C_{i-1}-{}^{\alpha}C_i$ axis into the plane perpendicular to this.

On averaging the spherical harmonics in the presence of Gaussian axial fluctuations about the *y*-axis (such that $\phi = 0$) of this frame, using[21]

$$\langle\cos(m\chi)\rangle = \int_{-\infty}^{\infty} d\chi\, p(\chi)\cos(m\chi) = e^{-m^2\sigma^2/2}\cos(m\chi_0)$$

where

$$p(\chi) = (2\pi\sigma_\chi^{\,2})^{-1/2} e^{-\chi^{2/(2\sigma^2)}} \quad (5)$$

(22) Fischer, M. W. F.; Zeng, L.; Pang, Y.; Hu, W.; Majumdar, A.; Zuiderweg, E. R. P. *J. Am. Chem. Soc.* **1997**, *119*, 12629−12642.
(23) Pang, Y.; Zuiderweg, E. R. P. *J. Am. Chem. Soc.* **2000**, *122*, 4841−4842.

and inserting these into eq 4, we can simply derive the following expression:

$$\langle D_{N-^{N}H}\rangle_{o-GAF} = -\frac{\gamma_i\gamma_j\mu_0 h}{16\pi^3 r^3}\left[\frac{A_a}{4}\{s_1(3\cos^2\beta - 1) + 3s_2\sin^2\beta\cos2\alpha\} + \frac{3}{8}A_r\left\{s_1\sin^2\beta\cos2\gamma + 2s_2\left(\cos^4\frac{\beta}{2}\cos2\delta_1 + \sin^4\frac{\beta}{2}\cos2\delta_2\right)\right\}\right] \quad (6)$$

with

$$\delta_1 = \alpha + \gamma; \quad \delta_2 = \alpha - \gamma; \quad s_1 = 1 + 3e^{-2\sigma^2}; \quad s_2 = 1 - e^{-2\sigma^2}$$

(α, β, γ) define the orientation of the local peptide plane frame relative to the tensor. By inspection, this reduces to eq 1 when $\sigma = 0$, with $\beta = \theta$ and $\gamma = \phi$. Under these conditions the measured coupling is independent of the orientation of the peptide plane relative to the $N-{}^{N}H$ vector (defined by the angle α_{pp}).

This description will be shown to be valid for the $N-{}^{N}H$ vector and can satisfactorily reproduce simulated 1D-GAF motional amplitudes, despite the fact that the rotational axis is actually tilted by 11° from the $^{\alpha}C_{i-1}-{}^{\alpha}C_i$ vector. We will call this motional model the ortho-1D GAF or o-GAF. We then define the average $N-{}^{N}H$ RDC measured under this motion $\langle D_{NH}\rangle_{o-GAF}$.

Methods

Gaussian Axial Fluctuation Monte Carlo Simulations and Analysis. The effect of the 3D-GAF motion on the RDCs was simulated for four different peptide plane vectors: $N-{}^{N}H$, $C'-{}^{N}H$, $^{\alpha}C-C'$, and $C'-N$, from the coordinates of the protein, the definition of the tensor (A_a, A_r, θ, ϕ, ψ) and the amplitudes of the 3D Gaussian fluctuations, σ_α, σ_β, and σ_γ. Unitary vectors joining desired spin pairs were submitted to three consecutive rotations around the 3D-GAF axes (see Introduction).[20] The normalized vector between $^{\alpha}C_{i-1}$ and $^{\alpha}C_i$ defines the axis γ, around which first 3D-GAF motion takes place. The angle of rotation of the $N-{}^{N}H$ vector around the $^{\alpha}C_{i-1}-{}^{\alpha}C_i$ vector is randomly chosen from a Gaussian distribution centered at 0.0 and with an amplitude of σ_γ. Resulting coordinates of the first GAF motion were rotated around the α axis, a vector in the peptide plane perpendicular to the $^{\alpha}C_{i-1}-{}^{\alpha}C_i$ axis. The extent of this rotation is extracted from a Gaussian distribution centered on 0.0 and with an amplitude of σ_α. The resulting coordinates were rotated a third time around the β axis, which lies perpendicular to the two previous axes, orthogonal to the peptide plane. The extent of this rotation comes from a Gaussian distribution of amplitude σ_β. Final coordinates were transformed into the alignment tensor principal axis system using the initially defined Euler angles and RDC values were calculated using the standard equation.[1] This process was repeated 50 000 times for every peptide plane of the protein. Amplitudes used for 3D-GAF Monte Carlo simulations were those obtained previously combining a long MD simulation and measured ^{15}N and $^{13}C'$ relaxation rates: $\sigma_\gamma = 16.6°$ and $\sigma_\alpha = \sigma_\beta = 6.7°$.[20] RDC values assuming no dynamic averaging (D_{stat}) were calculated from the protein coordinates and the appropriate definition of the tensor.

Generation of 1D-GAF conformations and RDC ensembles was performed using the same approach with $\sigma_\alpha = \sigma_\beta = 0$. A value of $\sigma_\gamma = 15°$ is used for all 1D-GAF Monte Carlo simulations. The average of those 50 000 RDCs generated is defined as D_{av}.

Site-specific effects of individual peptide plane motion on RDC averaging can be measured through the parameter Δ_{dyn}, the difference

between the RDC that one would expect if no dynamic process were present D_{stat}, and the averaged RDC from Monte Carlo simulations, D_{av}

$$\Delta_{dyn} = D_{stat} - D_{av} \quad (7)$$

The skewness parameter, *Sk*, was used for the analysis of the histograms of the accessible RDCs generated with the Monte Carlo simulation program. *Sk* describes the shape of a distribution with *N* members with respect to its average value $\langle D \rangle$:

$$Sk = \frac{1}{N}\sum_{j=1}^{N}[\{(D_j - \langle D \rangle)\}/\{\delta_D\}]^3 \quad (8)$$

Here δ_D is the standard deviation of the sampled RDC, D_j. A positive value of *Sk* implies an asymmetric distribution extending out toward more positive values of RDC, a negative value indicates the contrary. If the distribution is symmetric, $Sk = 0$.

Structural Models for SiR and MsrA and Experimental Data Sets. X-ray crystallographic structures of highly homologous molecules of the 18 kDa Flavodoxin-like domain of Sulfite reductase (FP18−SiR) have previously been used to model the structure of this protein on the basis of primary sequence,[24] this structure is again used here to represent the solution conformation. The methionine sulfoxide reductase structure from *Escherichia coli*[25] was used to represent the solution conformation of the molecule from *Erwinia chrysanthemi*.

For simulation purposes protein SiR was used and the Euler angles that define the alignment tensor in a bacteriophage Pf1 solution were used: $\theta = -59.85°$, $\phi = 97.60°$, and $\psi = 47.85°$.[24] This structure was refined to contain no energetically unfavorable definitions of peptide planes.

Backbone $N-^{N}H$ and $C'-^{\alpha}C$ RDC from these two molecules aligned in Pf1 bacteriophage[26] have previously been presented[24,27] and are used on the analysis presented here. Other published RDC data sets has been used in this work: ubiquitin in numerous different alignment media,[28−30] Protein G in five different alignment media,[18] dihydrofolate reductase[31] (DHFR) studied in bicelles and C12E5/hexanol mixture,[32] and lysozyme[33] studied in bicelles and bicelles doped with CTAB.[34] High-resolution X-ray structures have been used for the fitting of the alignment tensor for those data sets: 1ubq,[35] 1igd,[36] 3dfr,[37] and 3lzt[38] for ubiquitin, Protein G, DHFR, and lysozyme, respectively. A total of 12 additional X-ray and neutron diffraction structures were used to fit the lysozyme data to address the dependence of structure resolution on the behavior of the ortho-GAF approach: 1lks,[39] 193l,[40] 1hf4, [41]1aki, [42]1lkr, [39]1lzn,[43] 1lse,[44] 5lym,[45] 1fow,[46] 1lyz,[47] 1hsw,[48] and 1jpo.[49]

Determination of Alignment Tensors. The program Module[50] was used to fit alignment tensor parameters (A_a, A_r, θ, ϕ, ψ) for both experimental and simulated RDC data sets. Unless stated, vector distances: $N-^{N}H$, $^{\alpha}C-C'$, $C'-{}^{N}H$, and $C'-N$ were set to the values of 1.02, 1.53, 2.05, and 1.33 Å, respectively. Note that the $N-^{N}H$ distance of 1.04 Å, which is the motionally scaled value calibrated in an earlier study, is not used here unless otherwise stated. The reasons for this choice will become clear in the Results and Discussion section.

A modified version of the program Module has been used for the simultaneous determination of the amplitude of 1D-GAF motion, σ, and the alignment tensor parameters. This version of the program introduces the analytical equation that describes $N-^{N}H$ RDCs under an ortho-GAF motional regime (eq 6). In this case six parameters are extracted (A_a, A_r, θ, ϕ, ψ, σ). Simultaneous fitting of $N-^{N}H$ and $^{\alpha}C-C'$ RDCs measured in the same alignment medium has been also performed using the same modified version of Module.

The statistical significance of the fitting using the additional parameter σ, compared to the standard approach, is evaluated using standard *F*-test analysis, the parameter *p* indicates the probability that the improvement in the error using one additional parameter is due to random fluctuations.

Noise Simulations. Random structural noise was simulated using the same program as used for simulating the 3D-GAF, with three successive rotations of each individual $N-^{N}H$ vector around the α, β, and γ axes. In this case the amplitudes of the three rotations were varied randomly from Gaussian distributions of equal widths ϵ_{struc} centered at zero. Additional structural noise simulations used the same program as for simulating 1D-GAF, with one rotation of each individual $N-^{N}H$ vector around the $^{\alpha}C_{i-1}-^{\alpha}C_i$ axis. The amplitude of the rotation was varied randomly from a Gaussian distribution of width ϵ_{struc} centered at zero. A total of 100 different structures were generated for each simulation. Final results represent the average over this ensemble. Random noise was selected from a Gaussian distribution of width ϵ_{ran}.

Results and Discussion

The aim of this study was to determine the extent to which the Gaussian axial fluctuation (GAF) model for peptide plane backbone motion can be used to incorporate dynamic information into the analysis of dipolar couplings measured in weakly aligned proteins. To understand this we have undertaken a detailed characterization of the averaging behavior of backbone RDCs in the presence of these motions.

Averaging of RDCs in the Presence of Gaussian Axial Fluctuation Motion. In a first step, we simulated conformationally averaged $N-^{N}H$ RDCs (D_{av}) using the 18 kDa domain of sulfite reductase, assuming a one-dimensional GAF motion of amplitude ($\sigma = 15°$) about the $^{\alpha}C_{i-1}-^{\alpha}C_i$ axis at all $N-^{N}H$ sites. These are compared to values calculated assuming a static

(24) Champier, L.; Sibille, N.; Bersch, B.; Brutscher, B.; Blackledge, M.; Covès, J. *Biochemistry* **2002**, *41*, 3770−3780.
(25) Tete-Favier, F.; Cobessi, D.; Boschi-Muller, S.; Azza, S.; Branlant, G.; Aubry, A. *Structure* **2000**, *8*, 1167−1178.
(26) Hansen, M.; Mueller, L.; Pardi, A. *Nat. Struct. Biol.* **1998**, *5*, 1065−1071.
(27) Béraud, S.; Bersch, B.; Brutscher, B.; Gans, P.; Barras, F.; Blackledge, M. *J. Am. Chem. Soc.* **2002**, *124*, 13709−13715.
(28) Ottiger, M.; Bax, A. *J. Am. Chem. Soc.* **1998**, *120*, 12334−12341.
(29) Cornilescu, G.; Marquardt, J. L.; Ottiger, M.; Bax, A. *J. Am. Chem. Soc.* **1998**, *120*, 6836−6837.
(30) Hus, J.-C.; Peti, W.; Griesinger, C.; Brüschweiler, R. *J. Am. Chem. Soc.* **2003**, *125*, 5596−5597.
(31) Polshakov, V. I.; Smirnov, E. G.; Birdsall, B.; Kelly, G.; Feeney, J. *J. Biomol. NMR* **2002**, *24*, 67−70.
(32) Ruckert, M.; Otting, G. *J. Am. Chem. Soc.* **2000**, *122*, 7793−7794.
(33) Schwalbe, H.; Grimshaw, S. B.; Spencer, A.; Buck, M.; Boyd, J.; Dobson, C. M.; Redfield, C.; Smith, L. J. *Protein Sci.* **2001**, *10*, 677−688.
(34) Ramirez, B. A.; Bax, A. *J. Am. Chem. Soc.* **1998**, *120*, 9106−9107.
(35) Vijay-Kumar, S.; Bugg, C. E.; Cook, W. J. *J. Mol. Biol.* **1987**, *194*, 531−544.
(36) Derrick, J. P.; Wigley, D. B. *J. Mol. Biol.* **1994**, *243*, 906−918.
(37) Bolin, J. T.; Filman, D. J.; Matthews, D. A.; Hamlin, R. C.; Kraut, J. *J. Biol. Chem.* **1982**, *257*, 13650−13652.
(38) Walsh, M. A.; Schneider, T. R.; Sieker, L. C.; Dauter, Z.; Lamzin, V. S.; Wilson, K. S. *Acta Crystallogr. D.* **1998**, *54*, 522−546.
(39) Steinrauf, M. A. *Acta Crystallogr. D.* **1998**, *54*, 767−780.
(40) Vaney, M. C.; Maignan, S.; Riès-Kautt, M.; Ducruix, A. *Acta Crystallogr. D: Biol. Crystallogr.* **1996**, *52*, 505−517.
(41) Vaney, M. C.; Broutin, I.; Retailleau, P.; Douangamath, A.; Lafont, S.; Hamiaux, C.; Prange, T.; Ducruix, A.; Riès-Kautt, M. *Acta Crystallogr. D* **2001**, *57*, 929−940.
(42) Artymiuk, P. J.; Blake, C. C. F.; Rice, D. W.; Wilson, K. W. *Acta Crystallogr. B* **1982**, *38*, 778−788.
(43) Bon, C.; Lehmann, M. S.; Wilkinson, C. *Acta Crystallogr. D* **1999**, *55*, 978−987.
(44) Kurinov, I. V.; Harrison, R. W. *Acta Crystallogr. D* **1995**, *51*, 98−110.
(45) Sundaralingam, M.; Rao, S. RCSB Protein Data Bank, Deposition Date July 1995.
(46) Biswal, B. K.; Sukumar, N.; Vijayan, M. *Acta Crystallogr. D: Biol. Crystallogr.* **2000**, *56*, 1110−1119.
(47) Diamond, R. *J. Mol. Biol.* **1974**, *82*, 371−392.
(48) Sukumar, N.; Biswal, B. K.; Vijayan, M.:*Acta Crystallogr. D: Biol. Crystallogr.* **1999**, *55*, 934−937.
(49) Bradbrook, S.; Deacon, A.; Habash, J.; Helliwell, J. R.; Helliwell, M.; Nieh, Y. P.; Snell, E. H.; Trapani, G.; Thompson, A. W.; Campbell, J. W.; Allinson, N. M.; Moon, K.; Ursby, T.; Wulff, M. *Proc. SPIE-Int. Soc. Opt. Eng.* **1995**, *2521*, 160.
(50) Dosset, P.; Hus, J.-C.; Marion, D.; Blackledge, M. *J. Biomol. NMR* **2001**, *20*, 223−231.

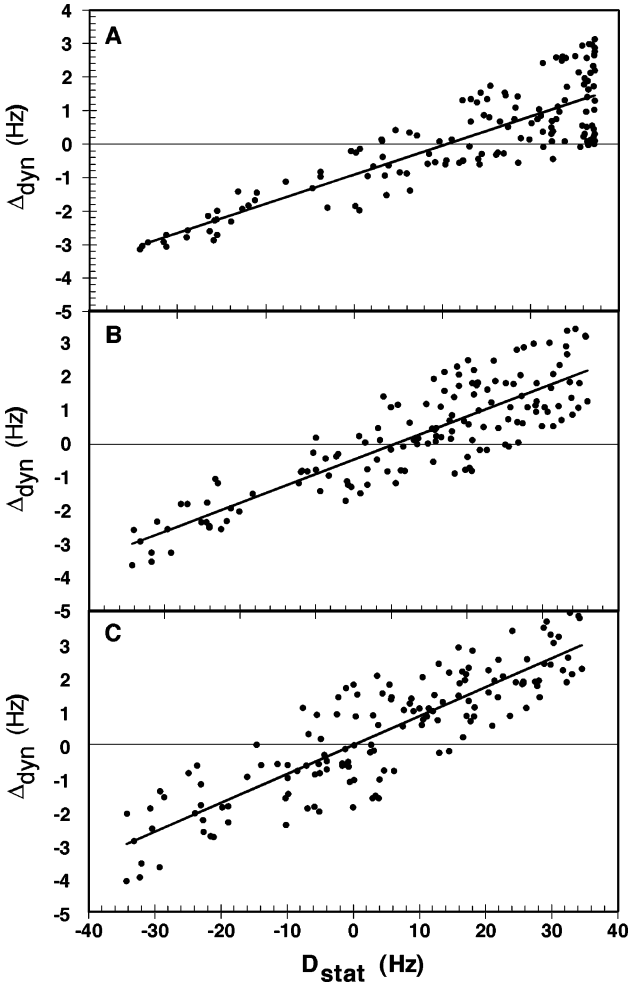

Figure 1. Effects of anisotropic peptide plane motion on average N−^{N}H RDC. Distribution of values of Δ_{dyn} ($D_{stat} - D_{av}$) with respect to D_{stat} calculated for 144 peptide planes distributed throughout the model protein SiR, assuming $\sigma = 15°$ 1D-GAF motion. Simulations were performed for different alignment tensors with (a) $A_r = 0$, (b) $A_r = A_a/3$, (c) $A_r = 2A_a/3$. Common value of $A_a = -16.0 \times 10^{-4}$ and Euler angles described in the Methods were used for simulations. Linear regressions are plotted as a solid line. No motion would result in a flat line at $\Delta_{dyn} = 0$, while cylindrically symmetric motion would give a linear relationship between Δ_{dyn} and D_{stat}.

model (D_{stat}). RDC averaging (measured by Δ_{dyn}, eq 7) in the 1D-GAF motional regime is found to vary considerably depending on the orientation of the peptide plane. This is illustrated in Figure 1, where equal amplitude motions are shown to result in very different scaling effects on the effective RDCs from different sites in the molecule (D_{stat}). These averaging effects can give higher, lower, or negligible effects on the RDC values compared to the static value, depending on the orientation of the peptide plane relative to the alignment tensor.

This is in contrast to the case of cylindrically symmetric motion of uniform amplitude, where RDC values would be scaled identically throughout the molecule, independent of the peptide plane orientation. If the amplitude of these motions is assumed to be uniform, Δ_{dyn} is a linear function of D_{stat} such that $\Delta_{dyn} = (1 - S^{ax})D_{stat}$, where S^{ax} is the order parameter common to all sites. Standard alignment tensor analyses, using a static model, implicitly make this assumption, and an average order parameter $\langle S^{ax} \rangle$ is effectively absorbed into the alignment tensor magnitude.

If a static tensor approach is applied to the analysis of 1D-GAF averaged data, for example to determine the alignment tensor from a known structure, the resulting values of A_a and A_r will also be scaled by an effective average order parameter $\langle S^{ax} \rangle$ relative to the true values. To illustrate this point we have fitted the dynamically averaged data, using a 1D-GAF amplitude of $\sigma = 15°$, to a static tensor using the program Module (Table 1). This yields values of A_a and A_r scaled by 0.91 (the Euler angles are more or less unchanged). The reasons for this become clear when we realize that this factor can also be extracted from the slope of Δ_{dyn} against D_{stat} for the distributions shown in Figure 1. This uniform scaling factor only partially accounts for the anisotropic dynamic component and leaves the remaining "scatter" to be interpreted as experimental noise, hence the high χ^2 value.

We have investigated the reasons for the inhomogeneous scaling of RDC in the presence of equal amplitude GAF-like motions in more detail by inspecting the distributions of sampled RDC with respect to the explored angles relative to the tensor. For the sake of simplicity we initially illustrate this behavior in the presence of an axially symmetric alignment tensor, so that the angular sampling can be expressed by a single parameter θ. RDC sampling for four differently oriented residues is shown in Figure 2.

The different behavior for these sites is evidently related not only to the average direction of the N−^{N}H vector of interest with respect to the alignment tensor, but also to the direction of the rotation axis $^{\alpha}C_{i-1}-^{\alpha}C_i$. This is exemplified in residues A68 and T71 which present almost equivalent static RDCs (16.78 and 16.98 Hz) but explore a very different range of RDCs, giving rise to very different Δ_{dyn} for the two vectors, (0.12 and 2.98 Hz). Figure 2 also shows RDC sampling for residues A68 and K109 for which the value of Δ_{dyn} is very small (0.12 and 0.04 Hz). For residue A68, there is almost no sampling of θ because the $^{\alpha}C_{i-1}-^{\alpha}C_i$ rotation axis is nearly parallel to the unique axis of the alignment tensor. The N−^{N}H bond therefore moves along an RDC−isocontour arc in the equatorial plane, sampling a very narrow distribution of RDCs. On the other hand, K109, whose peptide plane lies in the $x-y$ plane of the tensor, samples directions orthogonal to this, covering the full range of RDC, from +17 to −34 Hz. The very small value of Δ_{dyn} comes from the precise compensation of RDCs higher and lower than the static value and results in a nearly negligible shift compared to the static value. Residues showing sharp and asymmetric distributions of accessible RDCs tend, on the other hand, to derive from residues with large values of Δ_{dyn} (T71 and A80 in Figure 2 have Δ_{dyn} values of +2.98 and −3.14 Hz, respectively).

Asymmetry of RDC Sampling and Dynamic Averaging. The generality of the observation that nonuniform averaging effects are correlated with the symmetry of RDC sampling was examined by measuring the degree of asymmetry of the RDC distributions in terms of the skewness parameter *Sk* (see Methods). Figure 3 shows the parameter *Sk* for all residues of the model protein as a function of the absolute value Δ_{dyn} for three different degrees of rhombicity, assuming 1D-GAF motion. In general low values of $|\Delta_{dyn}|$ coincide with low values of skewness, characterizing essentially symmetric sampling. This confirms the general nature of the observation, illustrated for certain residues in Figure 2, that an asymmetric distribution of

Table 1. Analysis of N−^{N}H RDC

a. Analysis Using Static and Ortho-GAF Averaging Models[a]

data	fit	A_a (10^{-4})	σ (deg)	χ^2/N[e]	p[l]
simulated	static[c]	17.9		1.26	$<10^{-10}$
1D-GAF[a]	dyn[d]	19.4	14.3	0.083	
simulated	static	17.2		1.21	$<10^{-10}$
3D-GAF[b]	dyn	18.6	14.3	0.12	
SiR	static	17.5		5.58	0.035
(69)[f]	dyn	19.4	15.5	5.20	
MSR	static	14.7		2.59	0.02
(59)[g]	dyn	16.2	14.4	2.38	
DHFR	static	8.4		0.76	0.04
(82)[h]	dyn	9.1	12.8	0.71	
DHFR	static	9.1		1.7	0.05
(51)[i]	dyn	10.4	17.3	1.5	
ubiquitin	static	12.7		2.07	0.01
(61)[j]	dyn	13.8	14.7	1.85	
lysozyme Bic[k]	static	14.7		2.84	0.05
(ss − 52)	dyn	16.6	16.5	2.62	
lysozyme Bic	static	13.6		4.33	0.002
(loop 51)	dyn	16.5	19.6	4.00	
lysozyme Bic	static	14.1		3.25	0.0003
(all − 103)	dyn	16.4	17.9	2.89	
lysozyme ch Bic	static	11.9		2.03	0.03
(ss − 50)	dyn	13.5	17.0	1.81	
lysozyme ch Bic	static	10.9		1.93	0.001
(loop − 47)	dyn	13.2	20.1	1.50	
lysozyme ch Bic	static	11.3		2.05	0.000 09
(all − 97)	dyn	13.2	18.8	1.73	

b. Analysis of data from Lysozyme Aligned in Charged Bicelles Using 13 Different Structural Models[m]

resolution (Å)	fit	σ (deg)	χ^2/N	p[p]
0.9	static[n]		2.05	0.000 09
(3lzt)	dyn[o]	18.8	1.73	
1.1	static		1.40	0.000 01
(1lks)	dyn	17.4	1.14	
1.3	static		1.34	0.08
(193l)	dyn	12.1	1.29	
1.45	static		1.76	0.003
(1hf4)	dyn	16.0	1.60	
1.5	static		1.76	0.0005
(1aki)	dyn	17.2	1.54	
1.6	static		2.11	0.02
(1lkr)	dyn	14.9	1.99	
1.7	static		1.76	0.000 04
(1lzn)[q]	dyn	18.5	1.46	
1.7	static		2.57	0.01
(1lse)	dyn	16.0	2.41	
1.8	static		1.99	0.0006
(5lym)	dyn	17.5	1.74	
1.9	static		2.44	0.002
(1fow)	dyn	17.8	2.19	
2.0	static		8.72	0.13
(1lyz)	dyn	19.4	8.51	
2.0	static		2.26	0.004
(1hsw)	dyn	16.5	2.06	
2.1	static		1.93	0.0007
(1jpo)	dyn	17.2	1.70	

[a] 146 vectors were simulated using 50 000 Monte Carlo simulations of 1D-GAF motions about the $^{\alpha}C_{i-1}-^{\alpha}C_i$ axis ($\sigma = 15°$) using tensor ($A_a = 19.4 \times 10^{-4}$, $A_r = 12.9 \times 10^{-4}$, $\theta = -26°$, $\phi = 83°$, $\psi = 77°$). [b] 146 vectors were simulated using 50 000 Monte Carlo simulations of 3D-GAF motions ($\sigma_\alpha = \sigma_\beta = 6.7°$, $\sigma_\gamma = 16.6°$); same tensor as for footnote *a*. [c] Refers to fitting (A_a, A_r, θ, ϕ, ψ) assuming static structure. Fitted A_r, θ, ϕ, and ψ values are found in the Supporting Information. [d] Refers to fitting (A_a, A_r, θ, ϕ, ψ, σ) using eq 6. [e] Errors due to experimental and structural noise were combined to give a value of 2 Hz for all experimental data sets. [f] RDC measured from protein aligned in phage.[24] [g] RDC measured from protein aligned in phage.[27] [h] RDC measured from protein aligned in bicelles.[31] [i] RDC measured from protein aligned in C12E5/ethanol mixture.[31] [j] RDC measured from protein aligned in CHAPSO/DLPC/CTAB (10:50:1; 4%).[15] [k] All lysozyme data from ref 33. [l] Probability that the improvement in the fit is due to random fluctuation. [m] The same data set consisting of 97 RDCs measured in loops and secondary structural elements from lysozyme aligned in charged bicelles[33] were fitted to each of the structures listed using the dynamic and static models. [n] Refers to fitting (A_a, A_r,θ, ϕ, ψ) assuming static structure. [o] Refers to fitting (A_a, A_r, θ, ϕ, ψ, σ) using eq 6. [p] Probability that the improvement in the fit is due to random fluctuation. [q] Neutron diffraction structure (1lzn.pdb).

sampled RDC is responsible for dynamic averaging effects in this simple motional regime.

Selection of Optimal Residues for the Calculation of Alignment Tensor Parameters. Simulations of equal amplitude 1D-GAF peptide plane motions thus indicate a clear differential averaging behavior depending on the orientation of the peptide plane. These simulations also allow us to identify RDC distributions ($\Delta_{dyn} \approx 0$) that preserve D_{av} as a valid observable to be interpreted in terms of the "static" or nondynamically averaged tensor. In principle, always assuming the GAF model we have used is valid, these findings would allow us to select residues intelligently, to calculate the static alignment tensor more accurately. To test this approach we have selected those residues having the lowest values of $|\Delta_{dyn}|$ as derived from simulation, for the alignment tensor analysis. We can apply this selection procedure using the tensor derived from a standard, static analysis of experimental data because the Euler angles are not significantly affected when 1D-GAF averaged data are analyzed in this way. Eight data sets using this optimal sampling (OS) were created, using an increasingly higher threshold for Δ_{dyn}, until the whole data set was included. A series of 50 control data sets (RS) were also created for comparison with each of the OS data sets, using a random selection of the same number of vectors.

This analysis was performed using RDCs simulated from a known static structure, and using experimental RDCs from secondary structural elements from the same protein. This allows a comparison of expected behavior in the presence of 1D-GAF motion with the behavior of experimentally measured data for the same tensor and number and distribution of data points. Figure 4 shows the analysis for two different proteins, SiR and MsrA, both aligned in a bacteriophage solution. Values of A_a and A_r obtained when we fit the OS data sets, and the averaged values $\langle A_a \rangle$ and $\langle A_r \rangle$ over the RS sets are presented with respect to increasing number of selected residues. In the case of simulated data for both proteins, the values of A_a obtained with the most selective OS data set are close to the values used to simulate data and decrease systematically when more residues are added. This is expected, as the added residues are increasingly sensitive to dynamics (with higher Δ_{dyn} values) and this dynamic averaging is increasingly aliased into the tensor definition (vide supra). The randomly selected data sets give average $\langle A_a \rangle$ values that are lower and insensitive to the number of residues used. When we examine the experimental data from both proteins, the same trends are reproduced: the extracted A_a values are higher using those sites we predict to have less dynamically affected RDCs. The randomly selected data sets give a uniformly scaled $\langle A_a \rangle$, which is again essentially independent of the number of vectors included in the analysis.

The dependence of alignment tensor amplitude on the nature of the selected residues demonstrates that an artificial decrease of alignment tensor parameters will generally occur if GAF-

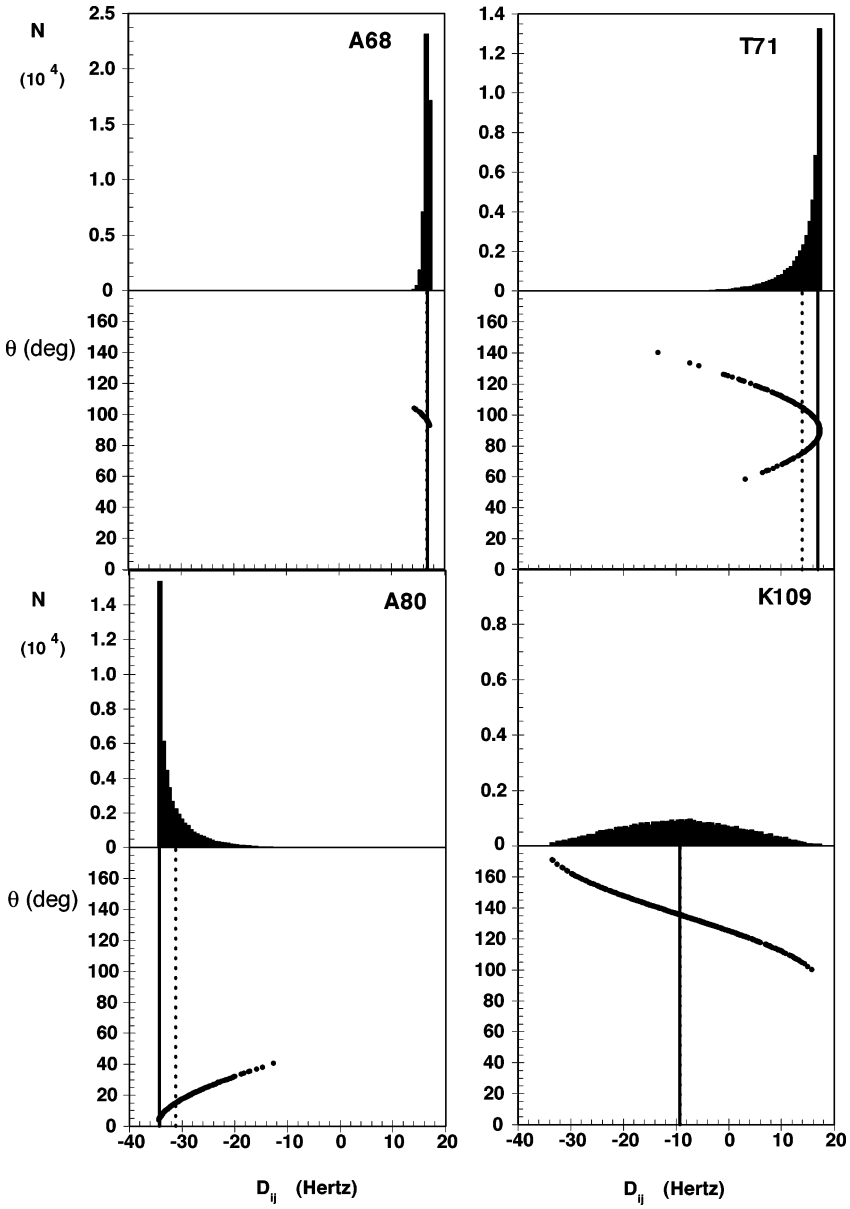

Figure 2. Angular sampling and N−^{N}H RDC distributions in the presence of anisotropic peptide plane motion. Histograms of accessible N−^{N}H RDCs and angular sampling for residues A68, T71, A80, and K109 assuming $\sigma = 15°$ 1D-GAF motion. Simulation of 50 000 peptide plane conformations from a Gaussian distribution centered around the static plane orientation was performed using the protein SiR. A definition of the alignment tensor is $A_a = -16.0 \times 10^{-4}$, $A_r = 0.0$, $\theta = -59.85°$, $\phi = 97.60°$, and $\psi = 47.85°$. Static, (D_{stat}) and averaged (D_{av}) values of RDC are plotted as solid and dashed vertical lines, respectively. For residues A68 and K109, D_{stat} and D_{av} lines are superimposed and cannot be distinguished.

like motions are present but are not specifically incorporated in the analysis and provides some evidence that these anisotropic motions are actually present. Other factors that can decrease alignment tensor parameter accuracy, for example experimental noise, would be expected to be of random nature, and this selection of residues would not be expected to yield the dependence observed here, as demonstrated by the insensitivity of the random selection.

Structural Noise Simulations. I. Underestimation of alignment tensor amplitudes has also been related to the presence of structural noise.[51] We have therefore explored the extent of these effects and compared them to those incurred due to anisotropic internal motion. To achieve this, exact data from the static model were fitted to structures with increasing amounts of structural noise (ϵ_{struct}), simulated randomly at all amide sites in the protein (see Methods). In Figure 5, values of A_a derived from this analysis and the associated χ^2 values are shown for simulations carried out using increasing amounts of structural noise. This behavior is compared to the value obtained when 1D-GAF simulated data (using $\sigma = 15°$) are fitted to the nonnoisy structure using the static model, as described in the preceding section. The results clearly show that high levels of structural noise must be present to match the scaling effects on the alignment tensor amplitude incurred due to 1D-GAF motion. With this amount of structural noise, the quality of the fitting ($\chi^2/N = 70.5$), is clearly unacceptable compared to the 1D-GAF simulated data, where low values of χ^2/N (0.86) are still obtained even for $\sigma = 15°$. This demonstrates that structural noise of this kind will not become a significant contributing factor to

(51) Zweckstetter, M.; Bax, A. *J. Biomol. NMR* **2002**, *23*, 127−137.

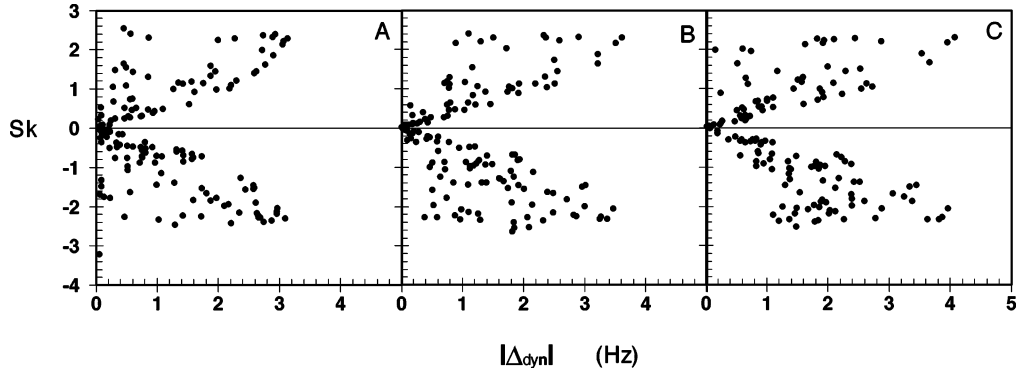

Figure 3. Effects of symmetry of RDC distribution on averaging. Relationship of $|\Delta_{dyn}|$ with the skewness parameter, *Sk*, for (a) $A_r = 0.0$, (b) $A_r = A_a/3$, and (c) $A_r = 2A_a/3$ for calculated for 144 peptide planes distributed throughout the model protein SiR, assuming $\sigma = 15°$ 1D-GAF motion. A total of 50 000 orientations were calculated from a Gaussian distribution centered around the static orientation. In all cases $A_a = -16.0 \times 10^{-4}$ and Euler angles specified in the Methods have been used.

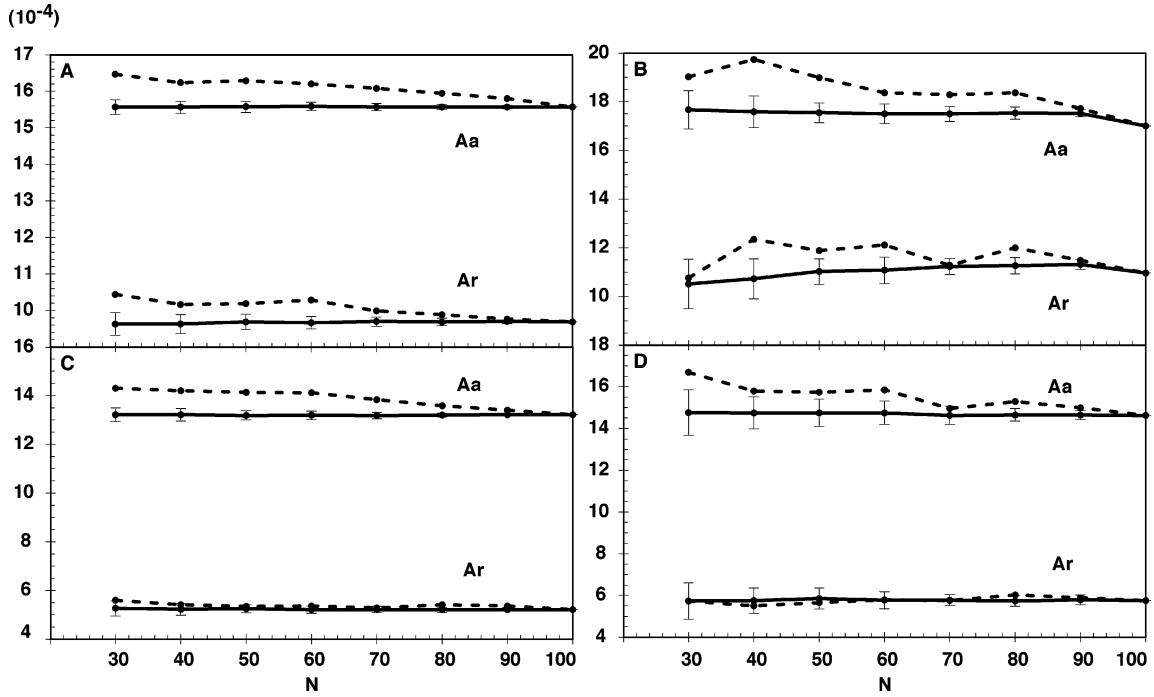

Figure 4. Selection of optimal $N-^{N}H$ vectors for the calculation of alignment tensor parameters: fitted A_a and A_r parameters (dashed lines) for optimally selected (OS) data sets; average fitted $\langle A_a \rangle$ and $\langle A_r \rangle$ (solid lines) for randomly selected (RS) data sets. OS data sets contain $N-^{N}H$ vectors with the lowest *N* values of Δ_{dyn}, while RS data sets contain *N* randomly selected $N-^{N}H$ vectors. This procedure was applied for simulated values of D_{ave} (A and C) and for experimental RDC (B and D), for proteins SiR (A and B) and MsrA (C and D). Note that the error bars correspond to the standard deviation of the 50 RS sets. Definition of the tensor obtained using the whole experimental RDC data set was used for the generation of the simulated D_{ave}.

alignment tensor scaling before the general fit quality will have deteriorated to an unacceptable level due to the same noise.

Direct Fitting of a Common Amplitude GAF Motion—Validation from Simulation. Selection of RDCs that can be predicted to be insensitive to GAF-like averaging can therefore be used in alignment tensor analysis to give a more precise definition of the tensor. A serious limitation of this approach is of course that the number of available RDCs is concomitantly reduced, and the uncertainty in the alignment tensor determination thereby increases. It would be more useful to include the anisotropic motion directly into the analytical expression for the RDC. As shown in Theory, it is simple to define the average coupling in the presence of an approximation to the 1D-GAF model, consisting of Gaussian axial fluctuations of amplitude σ around an axis perpendicular to the $N-^{N}H$ vector (ortho-GAF).

Before applying this to experimental data, the validity of this approximation was tested using numerical simulations of "true" 1D-GAF (about the $^{\alpha}C_{i-1}-^{\alpha}C$ axis) assuming a known static tensor. We used a modified Module algorithm to optimize (A_a, A_r, θ, ϕ, ψ, σ) and compared this analysis to the static model optimizing (A_a, A_r, θ, ϕ, ψ). Fitting the simulated dynamic data using the ortho-GAF model results in correct values of σ, A_a, and A_r and fits closely to the simulated data, validating the ability of the geometric model to describe true 1D-GAF motion (Table 1). As mentioned above the static model aliases the dynamic averaging effect into inaccurate static parameters, in particular systematically lower values for A_a and A_r. Not surprisingly the quality of the data reproduction using the ortho-GAF dynamic model, measured by the *p* value, reveals a highly significant improvement compared to the static model (Table 1; Supporting Information, Figure S1). It is worth noting that data simulated

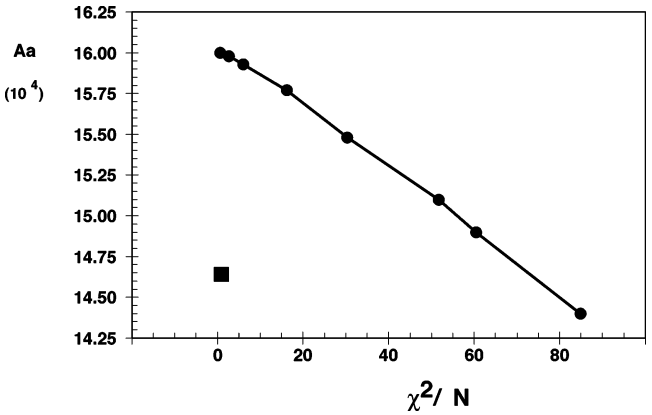

Figure 5. Effects of structural noise and GAF motions on A_a and quality of data fitting. Points (filled circles) on the line follow the extracted values of A_a (y-axis) and the equivalent reduced χ^2 value (x-axis), when exact data is fitted to structures with different degrees, of Gaussian structural noise (1, 2, 3, 4, 7, 9, 10, and 12°—see Methods). The square represents the value obtained when 1D-GAF (15°) data is fitted to model structure. Scaling of A_a equivalent to that experienced under $\sigma = 15°$ 1D-GAF motion would require structural noise leading to a very poor fit ($\chi^2/N > 70$). The model structure used was SiR, with A_a and A_r values of 16.0×10^{-4} and 10.6×10^{-4}.

using a cylindrically symmetric motion would give no improvement between the static and dynamic models, as this motion scales all RDC identically irrespective of the orientation with respect to the alignment tensor frame.

MD simulations suggest that true peptide plane motions may be more complicated than the 1D-GAF model, comprising additional, lower amplitude modes about axes orthogonal to the $^{\alpha}C_{i-1}-^{\alpha}C_i$ axis.[20] We have therefore simulated 3D-GAF motions assuming the amplitudes calibrated from relaxation data analysis,[20] and fitted these data to a static model and to eq 1 (Table 1; Supporting Information, Figure S1). The ortho-GAF analysis again extracts values of σ_{av}, A_a, and A_r that are close to the simulated values and fit the RDC significantly better than the static model.

Structural Noise Simulations. II. The possible effects of structural noise on this analysis were also tested: All $N-^{N}H$ vectors in the static SiR structure were reoriented either around randomly oriented axes or around the $^{\alpha}C_{i-1}-^{\alpha}C_i$ axis, in both cases by angles drawn from a Gaussian distribution of width $\epsilon_{struct} = 5°$ (see Methods). Data calculated from the static model were then fit to these 100 structures using the static and ortho-GAF models. No statistical improvement between the static and dynamic fits was found, while values of $\sigma_{av} < 1°$ were extracted. We conclude that structural noise is unlikely to alias into fictive motions. Notably for GAF-simulated data fitted to the same structure, correct σ values are still determined, demonstrating the robustness of the method with respect to this kind of error.

Direct Fitting of a Common Amplitude GAF Motion—Application to Experimental Data. In an initial application of this approach, we have extracted optimal average amplitudes of peptide plane motion using single-alignment medium $N-^{N}H$ RDC data from secondary structural elements in two proteins studied in our laboratory: methionine sulfoxide reductase (MsrA, 221 amino acids) and the 18 kDa domain of sulfite reductase (SiR, 165 amino acids), both aligned in bacteriophage solution. A significant reduction ($p < 0.05$) in the total χ^2 is found for both MsrA and SiR between the static and the ortho-GAF averaged model (Table 1). The optimal values for σ_{av} are similar and in the range of 15°. We have extended our analysis to a number of other published $N-^{N}H$ RDC data sets. In the case of dihydrofolate reductase (DHFR) aligned in two different alignment media, a significant improvement is detected using the anisotropic motional description for both data sets. Data from lysozyme, aligned in bicelles and in charged bicelles, again showed a highly significant improvement using this model compared to the static model, with a common amplitude of $\sigma_{av} = 16.5$ and 17.0° determined from the two independent analyses.

An exceptionally high-resolution crystal structure is available for the protein lysozyme[38] (0.92 Å), for this reason we have extended our analysis of these data to include the loop regions, which constitute approximately half of the structure. We find that the dynamic fits are again significantly better than the static model. The optimal average amplitude for the entire data set increases to $\sigma_{av} = 17.9$ and 18.8°, while use of only loop regions gives $\sigma_{av} = 19.6$ and 20.1°. It is worth noting that the alignment tensors components extracted from these analyses are similar, whereas the analysis using the static model gives different values for A_a and A_r depending on whether loops or secondary structure are used.

A value of σ_{av} in the range of 15° is thus found for secondary structural elements for all data sets where a significant improvement is observed on the basis of the p value. We have also replaced the imposed axis of rotation such that axes orthogonal to the $^{\alpha}C_{i-1}-^{\alpha}C$ direction (in the peptide plane or orthogonal to it) are used in the dynamically averaged model. Not surprisingly, we find no significant improvement in any of the tested data sets with respect to the static model, and σ_{av} values of $< 1°$ are found.

We have also assessed the possible reasons why an improvement may not be found for some data sets. In particular, we initially found no significant improvement for the molecule ubiquitin, despite apparently high measurement precision.[28] This lack of observable effects was tentatively ascribed to less complete sampling of orientational space by the different peptide planes present in the secondary structural elements present in this protein. This conclusion was supported by analysis of $N-^{N}H$ RDC from ubiquitin aligned in different media,[30] where significant improvement is indeed found (Table 1) using a data set sampling angular space more broadly than other data sets (Supporting Information, Figure S2). To characterize these effects more quantitatively, we have performed the following simulations.

Structural and Random Noise and Completeness of Angular Sampling. Increasing amounts of random noise (ϵ_{ran}) were added to simulated RDC under the influence of 1D-GAF in the presence of the five alignment tensors corresponding to the five best-fitting data sets used in the recently published study of ubiquitin.[15,30] Structural noise ($\epsilon_{struct} = 5°$) was again randomly added to the ^{N}H and N coordinates of the protein to create 100 structures. The noisy data from the five different tensors were fit to these structures using the static and dynamic models presented above. Figure 6 shows the dependence of p (the probability that the fit improvement is due to noise), and $\delta(\sigma)$ (the standard deviation of the derived σ values, essentially the precision with which this can be determined) for the five alignment tensors with respect to simulated random noise levels. This reveals that different angular sampling and alignment tensor amplitudes result in a significantly differing ability to character-

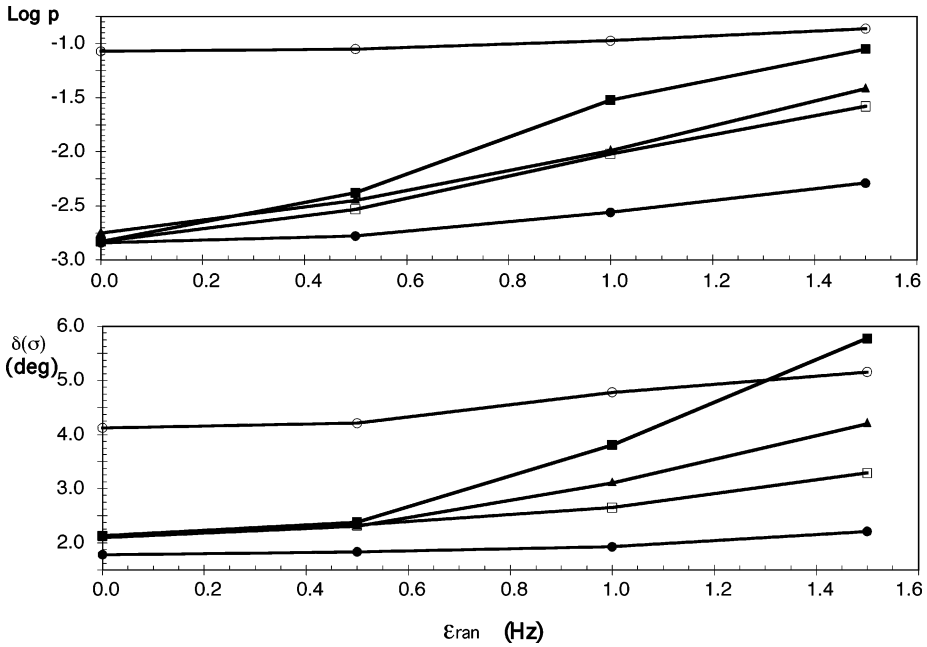

Figure 6. Effects of random and structural noise on fitting GAF motion using different alignment tensors for the protein ubiquitin. Data were simulated using $\sigma = 15°$ 1D-GAF motion in the presence of increasing levels of random noise (ϵ_{ran}) from 0 to 1.5 Hz, using the best fitting alignment tensors derived from the original experimental data sets.[15,31] These data were fit to 100 structures, each containing $\epsilon_{struct} = 5°$ structural noise. The ability of these data sets to detect the GAF motion is characterized by the average value of log(p), a measure of the significance of the improvement in the data fitting when using the GAF model compared to the static model, and $\delta(\sigma)$ the standard deviation of the extracted amplitude of the motion. Filled circles represent data simulated using the tensor derived from CHAPSO/DPLC/CTAB (10:50:1); filled squares represent data simulated using the tensor derived from Chapso DPLC; filled triangles represent data simulated using the tensor derived from (*n*-C12E5/hexanol); empty circles represent data simulated using the tensor derived from Pf1 phage; empty squares represent data simulated using the tensor derived from Bicelles. Notably the data set that fits best in the presence of noise (CHAPSO/DPLC/CTAB) corresponds to the experimental data set that gives a significant improvement using the GAF model.

ize σ_{av} in the presence of the same levels of noise. It is of particular interest to note that the simulated data set that provides the best characterization of σ (the lower lines in each plot) corresponds to the only experimental data of the five that actually gives a significant improvement using the dynamic model. This demonstrates the sensitivity of this technique to the combination of low levels of angular sampling and low levels of alignment, in the presence of imprecision, even for simulated data. Without going any further in this analysis, this already identifies a possible reason for the lack of significant improvement in some data sets from small proteins.

Effects of Structural Resolution on Extracted Dynamic Parameters. The precision of the coordinates of the protein structure is clearly a potentially important factor affecting the analysis of dynamics from this technique. To characterize these effects, we have analyzed data from 13 X-ray and neutron crystallographic structures of hen egg white lysozyme at different diffraction resolutions ranging from 0.9 to 2.1Å and compared their fitting characteristics. The results, shown in Table 1b, suggest that the technique is largely robust with respect to structural resolution. All analyses showing statistically significant improvement to a level of $p \leq 0.05$, comparing the fit using the dynamic model with the static model, extract similar values for σ (17.1 ± 1.1°, in a range from 14.9 to 18.8°) and show no detectable dependence on crystal diffraction resolution. Two fits do not give a significant improvement in the fit, and the σ values should therefore not be interpreted as physically meaningful (these values are $\sigma = 12°$ and 19°). It is of interest to note that the resolutions of these two structures are very different (1.3 and 2.0 Å), and that the structure with the lowest resolution (2.1 Å) exhibits both low χ^2 and low p value (0.0007) between the two models. The reproducibility of GAF amplitudes from the different structures is reassuring for the validity of this analysis; in particular, we note the convergence of σ values for those fits in which one can have most confidence as judged by the statistical testing procedure described here. Interestingly the neutron diffraction structure,[43] which is the only study to report explicitly on amide proton position (or in this case deuteron) also fits the data to high precision and resolves a highly significant improvement using the dynamic model.

Sensitivity of Different Peptide Plane RDCs to GAF Motions. Up to this point we have addressed the effects of dynamic motions on $N-^{N}H$ RDCs. In the following, we explore the dynamic averaging effects of 1D- and then 3D-GAF motions on commonly measured RDCs from additional spin-pairs in the peptide plane. Distributions of sampled RDC for different couplings belonging to the same peptide plane ($N-^{N}H$, $C'-^{N}H$, $^{\alpha}C-C'$, and $C'-N$) are shown in Figure 7a for 1D-GAF and 3D-GAF motional models. Averaging behavior of RDCs in the same plane is found to be heterogeneous, depending on the orientation of the plane with respect to the alignment tensor. 3D-GAF histograms are in general smoother than 1D-GAF sampling and in all cases sample a broader spectrum of RDCs. Further inspection of 3D-GAF histograms reveals that 46 $N-^{N}H$ vectors out of 146 (31%), explore more than the 90% of the whole RDC range, while this figure is only 3% of $^{\alpha}C-C'$, 15% of $C'-^{N}H$, and 10% of $C'-N$ couplings.

Figure 7c shows the normalized absolute values of Δ_{dyn} along the sequence for the four kinds of peptide plane RDCs in the presence of 1D-GAF motions. $N-^{N}H$ RDC are clearly the most affected by this kind of averaging, followed by the $C'-^{N}H$, $C'-N$, and finally the $^{\alpha}C-C'$ coupling which shows the lowest values of Δ_{dyn}. This differential behavior is of course determined by the geometry of the peptide plane that defines the orientation

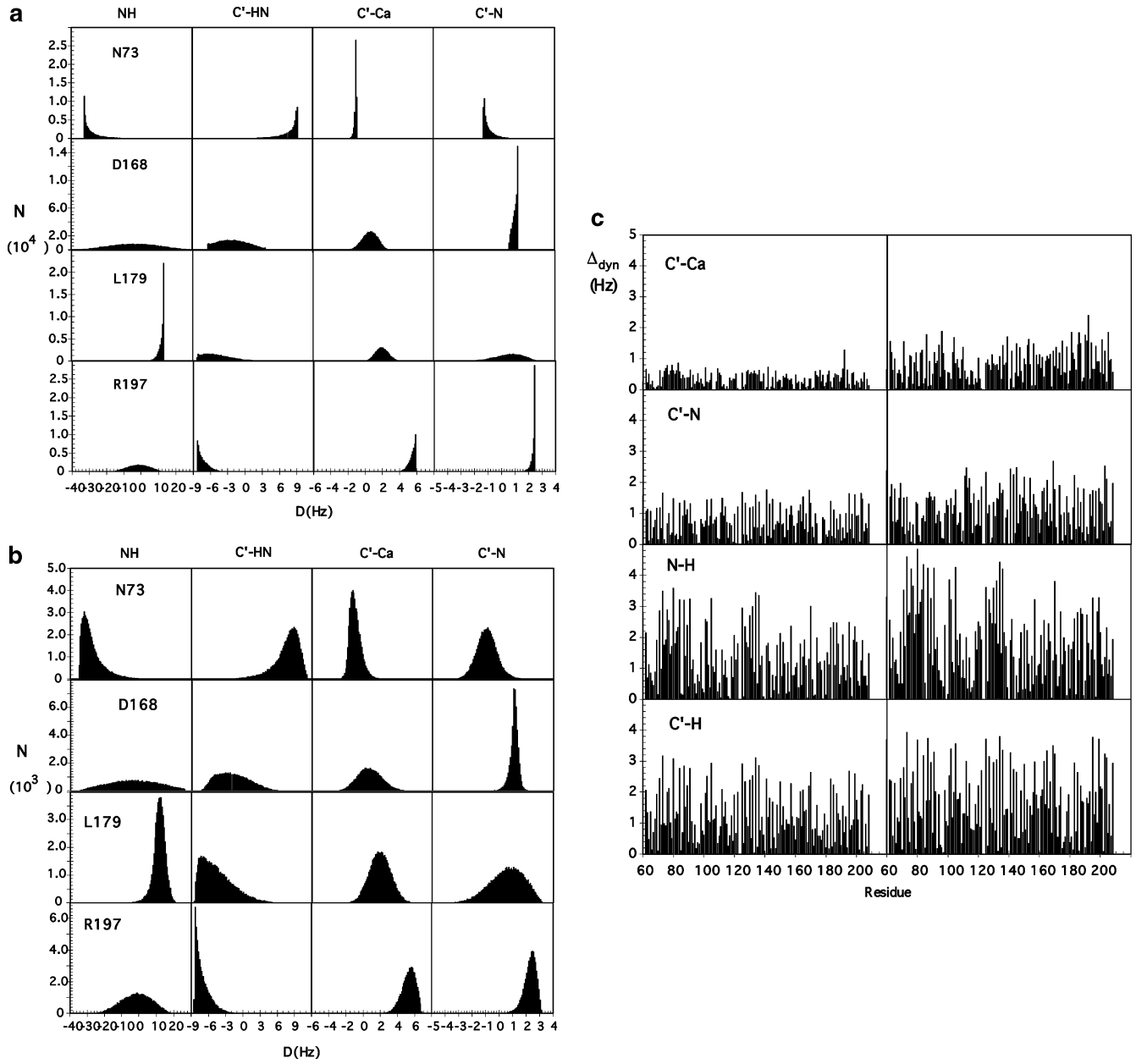

Figure 7. Sampling characteristics of different backbone vectors in the presence of 1D and 3D GAF motions. a. Histograms of accessible values of RDCs in a 1D-GAF (15°) dynamic regime in SiR. From top to bottom: panels corresponding to residues N73, D168, L179, and R197. Histograms corresponding to $N-^{N}H$, $C'-HN$, $^{\alpha}C-C'$, and $C'-N$ distributions are shown. Simulations were performed using $A_a = -16.0 \times 10^{-4}$, $A_r = A_a/3$, and Euler angles defined in the Methods. b. Histograms of accessible values of RDCs in a 3D-GAF dynamic regime in SiR. From top to bottom: panels corresponding to residues N73, D168, L179, and R197. Histograms corresponding to $N-^{N}H$, $C'-HN$, $^{\alpha}C-C'$, and $C'-N$ distributions are shown. Simulations were again performed using $A_a = -16.0 \times 10^{-4}$, $A_r = A_a/3$, and Euler angles defined in the Methods. c. Normalized absolute values of Δ_{dyn}. Left (right) panels correspond to the 1D-GAF (3D-GAF) model. Simulations again used the SiR structural model with $A_r = A_a/3$ and tensor definition specified in the Methods.

of each vector with respect to the $^{\alpha}C_{i-1}-^{\alpha}C_i$ axis (79, 67, 42, and 12° for $N-^{N}H$, $C'-^{N}H$, $C'-N$, and $^{\alpha}C-C'$ vectors respectively). Figure 7c also shows the systematic increase in the absolute values of Δ_{dyn} from 1D- to 3D-GAF due to the two additional reorientation modes. Peptide plane rotations around the β axis affect all vectors in the same way, as the β axis is perpendicular to the plane, while sensitivity of different RDCs with respect to rotations around the α axis are the inverse of those around the major axis (γ), so that the $N-^{N}H$ vector is the most insensitive and the $^{\alpha}C-C'$ vector the most sensitive. In both 1D- and 3D-GAF motional regimes, assuming the amplitudes used in the simulation are reasonable, the $^{\alpha}C-C'$ RDC is the least affected by dynamic averaging, and we would therefore expect this coupling to provide the most accurate determination of static tensor parameters.

Alignment Tensor Determination Using Different Backbone RDCs. The effect of dynamic averaging on alignment tensor determination was again characterized by fitting 1D- and 3D-GAF averaged RDCs to the static structure from which they were created. Results of the fitted parameters compared with those used as input for the simulation are shown in Table 2. This again demonstrates that GAF-averaged RDCs always yield smaller fitted parameters than those used to generate the data, although these effects are very different depending on the type of RDC. In the 1D-GAF model, A_a values are underestimated by 8.8%, 7.9%, 4.3%, and 1.3% for $N-^{N}H$, $C'-^{N}H$, $C'-N$, and

Table 2. Fitted Tensor Parameters for 1D- and 3D-GAF Simulated Data[a] Using the Static Tensor Model

	A_a^{theo} (10^{-4})	A_r^{theo} (10^{-4})	A_a^{all} (10^{-4}) (χ^2)	A_r^{all} (10^{-4})	A_a^{NH} (10^{-4}) (χ^2)	A_r^{NH} (10^{-4})	A_a^{CH} (10^{-4}) (χ^2)	A_r^{CH} (10^{-4})	A_a^{CC} (10^{-4}) (χ^2)	A_r^{CC} (10^{-4})	A_a^{CN} (10^{-4}) (χ^2)	A_r^{CN} (10^{-4})
1D[b]-GAF	−16.00	0.00	−14.67 (473)	−0.12	−14.60 (390)	−0.13	−14.74 (37.2)	−0.23	−15.80 (2.27)	−0.04	−15.32 (2.47)	−0.12
	−16.00	−5.33	−14.67 (470)	−4.96	−14.60 (388)	−4.96	−14.78 (39.9)	−5.00	−15.80 (2.55)	−5.27	−15.34 (2.71)	−5.08
	−16.00	−10.67	−14.70 (563)	−9.77	−14.64 (451)	−9.71	−14.82 (48.5)	−9.83	−15.81 (3.33)	−10.52	−15.36 (3.51)	−10.16
3D[c]-GAF	−16.00	0.00	−14.05 (445)	−0.12	−13.97 (364)	−0.13	−14.13 (34.5)	−0.27	−15.17 (2.58)	−0.05	−14.72 (2.31)	−0.19
	−16.00	−5.33	−14.06 (456)	−4.76	−13.99 (368)	−4.75	−14.18 (36.8)	−4.80	−15.18 (2.62)	−5.06	−14.75 (2.51)	−4.90
	−16.00	−10.67	−14.08 (541)	−9.38	−14.03 (435)	−9.31	−14.23 (44.8)	−9.42	−15.20 (3.01)	−10.08	−14.78 (3.19)	−9.75

[a] Average values of backbone RDC for the different coupling types were simulated from 50000 Monte Carlo simulations using tensor (A_a^{theo}, A_r^{theo})and Euler angle definition specified in the Methods. An uncertainty of 0.5 Hz for all couplings has been used for data fitting. [b] Monte Carlo simulations of 1D-GAF motions about the $^{\alpha}C_{i-1}-^{\alpha}C_i$ axis ($\sigma = 15°$). [c] Monte Carlo simulations of 3D-GAF motions ($\sigma_\alpha = \sigma_\beta = 6.7°$, $\sigma_\gamma = 16.6°$).

$^{\alpha}C-C'$ RDC, respectively. The same order is found for the 3D-GAF dynamic models, where underestimation of A_a fitted parameters are 12.7%, 11.7%, 8.0%, and 5.2% for $N-^{N}H$, $C'-^{N}H$, $C'-N$, and $^{\alpha}C-C'$ respectively. Again the rhombicity (defined as A_r/A_a) and the Euler angles (θ, ϕ, ψ) are essentially unaffected by these averaging effects. It is also clear from Table 2 that the highest values of the error function χ^2 correspond in all cases to the $N-^{N}H$ fitting, while $^{\alpha}C-C'$ and $C'-N$ RDCs yield much higher precision fits to the structural model.

The generally used $N-^{N}H$ bond length, $r_{NH} = 1.041 \pm 0.006$ Å was determined from calibration compared to RDCs measured between heavy atoms[29] and represents the vibrationally corrected average.[52] The authors of the earlier calibration study[29] suggested that $N-^{N}H$ specific motions were partially responsible for the unexpectedly long value for this distance compared to values commonly used, for example in ^{15}N relaxation and neutron diffraction studies.[53] We can investigate to what extent common GAF-like motions could account for this distance scaling using the results in Table 2. The ratio of effective alignment tensor values ($A_{a,NH}/A_{a,C'C\alpha}$) for a 1D-GAF motional amplitude of $\sigma = 15°$ gives a factor of 1.08, equivalent to a distance scaling of 1.026. Assuming a static value of 1.02 Å, the motionally scaled value would then be 1.046 Å, confirming that a value of σ in this range could account for the distance calibration determined in the earlier study.

Experimental Alignment Tensor Determination Using Different Backbone RDCs. Simulations introduced above indicate a differential accuracy in the prediction of alignment tensor parameters for diverse peptide plane vectors, due to different sensitivities to anisotropic dynamic averaging. To determine whether we could detect the largest expected differences from simulation (between $^{\alpha}C-C'$ and $N-^{N}H$ couplings), we have fitted data sets from different experimental systems using the static model (Table 3). In agreement with predicted effects, systematically higher values of A_a are extracted from $^{\alpha}C-C'$ RDCs fitting compared to those from other kinds of vectors. It is however impossible from this analysis to separate the scaling effects due to dynamic sampling from scaling incurred due to the choice of optimal internuclear distance. It is possibly worth noting that if we use the motionally scaled distance of 1.04 Å (vide supra) A_a values derived from $^{\alpha}C-C'$ couplings are slightly (4%) higher than those derived from $N-^{N}H$.

Table 3. Comparison of Extracted Alignment Tensor Parameters Using the Static Model[a] from Experimental $N-^{N}H$ and $^{\alpha}C-C'$ RDC

data set	A_a^{NH} (10^{-4})	A_r^{NH} (10^{-4})	A_a^{CC} (10^{-4})	A_r^{CC} (10^{-4})
	χ^2		χ^2	
SiR[b] (phage)	−15.99 ± 0.05	−10.49 ± 0.08	−16.88 ± 0.33	−11.22 ± 0.30
	1984		62	
MsrA[c] (phage)	13.80 ± 0.07	5.51 ± 0.07	14.33 ± 0.14	5.04 ± 0.16
	882		48	
protein G[d] (bicelles)	−13.62 ± 0.11	−4.06 ± 0.13	−15.09 ± 0.39	−3.95 ± 0.60
	478.4		39.1	
protein G[d] (alcohol)	−7.40 ± 0.09	−1.80 ± 0.10	−8.56 ± 0.44	−2.23 ± 0.65
	162.1		15.6	
protein G[d] (phage)	11.37 ± 0.09	1.24 ± 0.09	13.45 ± 0.41	1.31 ± 0.48
	565.8		20.4	
protein G[d] (neg. gels)	9.62 ± 0.10	4.52 ± 0.10	10.87 ± 0.38	4.57 ± 0.51
	420.1		13.9	
protein G[d] (pos. gels)	9.08 ± 0.07	5.62 ± 0.14	9.99 ± 0.41	6.19 ± 0.41
	397.2		17.7	

[a] Refers to fitting (A_a, A_r, θ, ϕ, ψ) assuming static structure. Fitted A_r,θ, ϕ, and ψ values are found in the Supporting Information. [b] Data from ref 24. [c] Data from ref 27. [d] Data from ref 18.

The χ^2 values in Table 3 indicate that significantly higher quality fitting is obtained using $^{\alpha}C-C'$ RDCs than $N-^{N}H$, assuming the same experimental precision. While this is also predicted from the 1D- and 3D-GAF simulated data (Table 2), the range of RDC must be taken into consideration when comparing relative χ^2 values, due to the effects of any kind of structural imprecision or dynamic processes on the different RDCs. For example an orientational error of 1° in the model structure will induce a more than five times greater difference in hertz for a calculated $N-^{N}H$ RDC than for a $^{\alpha}C-C'$ RDC. The resulting contribution to the total χ^2 value will then be 25 times greater assuming the same error. From the simulated 3D-GAF data, a ratio of χ^2 from $N-^{N}H$ and $^{\alpha}C-C'$ RDC of 145 is found, significantly greater than the value expected simply on the basis of the RDC range. In the case of experimental data (Table 3) the ratio is 21.7 ± 7.9, which is close to that which we might expect simply due to the different dynamic ranges of the two couplings.

This implies that the uncertainty in the fitting process is dominated by either structural noise or dynamics, both of which are sources of systematic error if interpreted using a static model. It is however impossible to distinguish between these effects

(52) Case, D. *J. Biomol. NMR.* **1999**, *15*, 95−102.
(53) Kvick, A.; Al-Karaghonli, A. R.; Koetzle, T. F, *Acta Crystallogr.* **1977**, *B33*, 3796−3802.

unless they are taken into consideration specifically in the fitting process. For this reason, we have developed the following approach to fitting $^{\alpha}C-C'$ and the $N-^{N}H$ RDC simultaneously to a common 3D-GAF motion.

Combined Description of 3D-GAF Motion for N—^{N}H and C′—$^{\alpha}$C RDC. We demonstrated above that a simple analytical approximation of motionally averaged $N-^{N}H$ RDC (ortho-GAF) can be used to approximately model data simulated using all three components of the more complex motion, containing smaller amplitude rotations about axes orthogonal to the $^{\alpha}C_{i-1}-^{\alpha}C_i$ axis (3D-GAF). Here we take this approach one step further and model 3D-GAF data simulated from different backbone RDCs using a combination of the analytical 1D-GAF motion and an additional axially symmetric component to the motion introduced to represent the averaging effects of the remaining equal amplitude modes. This axially symmetric component scales RDCs uniformly, independent of their direction and is equated here to the simple order parameter S_{ij}^{ax} introduced earlier. The aim here is to test whether the two additional small rotational motions in the directions orthogonal to the 1D-GAF motion (γ axis) can be absorbed into a general parametrized scaling factor. We have tested this model, by comparing the data numerically simulated using 3D-GAF motions, to an analytically calculated dipolar coupling $\langle D_{N-^{N}H}\rangle_{3DGAF}$ containing a single axially symmetric scaling term $S_{N-^{N}H}^{ax}$, and the single anisotropic motional term $\langle D_{N-^{N}H}\rangle_{o-GAF}$, defined in eq 6.

This can be expressed as follows:

$$\langle D_{N-^{N}H}\rangle_{3DGAF} = S_{N-^{N}H}^{ax}\langle D_{N-^{N}H}\rangle_{o-GAF} \quad (9)$$

The results (not shown) closely reproduce the numerically simulated values, demonstrating, perhaps not surprisingly, that, in the case of 3D-GAF motions where the two additional reorientation amplitudes are similar and small compared to the $N-^{N}H$ motion, the latter dominates the anisotropic nature of the motion. The scaling parameter $S_{N-^{N}H}^{ax}$ can be optimized in this fit to bring the slope equal to 1.

Similarly we have compared the $C'-^{\alpha}C$ RDC calculated from the numerical 3D-GAF simulation with a simple axially symmetric model assuming a negligible anisotropic component, $\langle D_{C'-^{\alpha}C}\rangle_{3DGAF}$:

$$\langle D_{C'-^{\alpha}C}\rangle_{3DGAF} \approx S_{C'-^{\alpha}C}^{ax}K_0^{C'-^{\alpha}C}\left[A_a(3\cos^2\theta - 1) + \frac{3}{2}A_r\sin^2\theta\cos 2\phi\right] \quad (10)$$

The results again closely reproduce the numerical simulations (results not shown). $S_{C'-^{\alpha}C}^{ax}$ can again be optimized to make the slope equal to 1. The values of $S_{N-^{N}H}^{ax}$ and $S_{C'-^{\alpha}C}^{ax}$ are very similar (0.96 and 0.95 respectively) and would correspond to axially symmetric motions in a cone of half-angle 9.4−10.5°. The similarity of the RDCs calculated using the 3D-GAF simulations and the two models, suggests that for these two backbone RDCs simple analytical definitions (eqs 9 and 10) can be safely used to model averaged RDCs in the presence of the complete 3D-GAF motion.

Simultaneous dynamic fitting of $N-^{N}H$ and $^{\alpha}C-C'$ RDCs. $N-^{N}H$ and $^{\alpha}C-C'$ RDCs were simultaneously fitted to eqs 9 and 10 to determine average amplitudes for the anisotropic motion. Initially only data from secondary structural elements were used. This strategy was applied to proteins SiR and MsrA aligned in bacteriophage Pf1, both studied in our laboratory, offering excellent sampling of angular space in both $N-^{N}H$ and $^{\alpha}C-C'$ coupling data sets. In comparison to the fit using only $N-^{N}H$ RDC the addition of $^{\alpha}C-C'$ data results in a similar average amplitude of anisotropic motion of $\sigma_{av} = 14.5°$ and $\sigma_{av} = 14.4°$ for SiR and MsrA respectively (Table 4). Moreover, p values decreased to 0.003 and 0.002 respectively, demonstrating that this model for anisotropic motion is able to reproduce both $N-^{N}H$ and $^{\alpha}C-C'$ couplings simultaneously and thereby provide an improved definition of the alignment tensor.

Table 4. Alignment Tensor Determination Using Simultaneous Analysis of $N-^{N}H$ and $^{\alpha}C-C'$ RDC from Static and Ortho-GAF Averaging Models[a]

data	fit	A_a (10^{-4})	A_r (10^{-4})	σ (deg)	p[e]
SiR (phage)[b]	static	−16.58	−10.71		0.003
70 + 67	dyn	−18.18	−12.08	14.97	
MSR (phage)[c]	static	13.83	5.52		0.002
69 + 74	dynamic	15.12	6.04	14.76	
protein G (C12E5/hex.)[d]	static	−7.55	−1.80		0.001
50 + 46	dynamic	−8.08	−1.91	14.75	
protein G (bicelles)	static	−13.92	−3.53		0.04
51 + 43	dynamic	−14.48	−3.84	12.05	
protein G (PG-Gel)	static	9.16	5.76		0.05
50 + 46	dynamic	9.57	5.93	11.30	
protein G (phage)	static	11.55	1.26		0.009
49 + 46	dynamic	12.26	1.37	13.64	

[a] Data fit to (A_a, A_r, θ, ϕ, ψ, σ) using eq 9 and 10 simultaneously. Fitted A_r,θ, ϕ, and ψ values are found in the Supporting Information. [b] Data from ref 24. [c] Data from ref 27. [d] Data from ref 18. [e] Probability that the improvement in the fit is due to random fluctuation.

One potential advantage of the simultaneous fitting of multiple couplings is the increased sampling of angular space compared to that covered by $N-^{N}H$ vectors in small proteins. We have therefore also applied this approach to the recently published backbone RDC data measured from protein G.[18] The five data sets containing only $N-^{N}H$ RDC from this small protein showed no statistical improvement using the ortho-GAF model, an effect possibly due to the small number of sites available in secondary structural elements (vide supra). In the case of $N-^{N}H/^{\alpha}C-C'$ fitting, four of the five data sets yield a statistically significant improvement compared to static fitting analysis (Table 4), with average dynamic amplitudes of σ_{av} of 14.8, 12.1, 11.3, and 13.6°, with a higher significance for the former and latter data sets, based on statistical characteristics. Note that using a lower resolution crystal structure of 2.1 Å (pdb reference 1pga) [54] motional amplitudes of 15.5, 12.2, and 14.8° are extracted from the same data sets for the three alignment media giving statistically significant improvement ($p = 0.004$, 0.04, and 0.001 for the alcohol, bicelle, and pc-gel mixtures respectively), underlining the robustness of this approach with respect to crystallographic resolution noted above for lysozyme.

The average amplitude of the detected motions is therefore essentially reproduced in four independent alignment systems for the same molecule. In addition average motional amplitudes determined from two larger proteins from our laboratory reproduce the observations derived from $N-^{N}H$ vectors alone. This combined approach to fitting $N-^{N}H$ and $^{\alpha}C-C'$ RDC therefore substantiates the results of our analysis of $N-^{N}H$ alone.

(54) Gallagher, T.; Alexander, P.; Bryan, P.; Gilliland, G. L. *Biochemistry* **1994**, *33* 4721.

Conclusions

Anisotropic reorientational modes of peptide planes have been evidenced using long MD simulations and relaxation rate analysis.[19,20,22,23] Here we have assessed the potential of using this geometric model for peptide plane reorientation to analyze and extract dynamic information from dipolar couplings measured in weakly aligned samples. From simulation, we find that these motions differentially affect measured RDCs, depending on the orientation of the peptide plane in the principal axis system of the alignment tensor, and therefore affect apparent tensor parameters extracted from these data. The consequences of this orientation-dependent scaling on alignment tensor determination have been simulated, and expected effects have been reproduced in experimental data from diverse proteins. This already provides evidence for the existence of GAF-like motions in proteins. To study this further we have developed an approximate analytical definition of averaged RDC under the influence of a simple GAF-like motion.

This description allows the incorporation of an average peptide plane reorientation amplitude (σ_{av}) into alignment tensor analysis using single-medium $N-^{N}H$ RDC data sets. Application to secondary structural elements from five different proteins detects significantly improves descriptions of the alignment tensors, and determines optimum σ_{av} values ranging from 14.4 to 17.0° for the different proteins. While the assumption of common amplitude motions in secondary structure is an approximation, this average amplitude is quite closely reproduced between the different proteins studied here, and we note that the similarity with results from a detailed analysis of $^{13}C/^{15}N$ spin relaxation data in terms of the 3D-GAF model ($\sigma_{av} \approx 16°$).[20] For one protein with an exceptionally high-resolution crystal structure (lysozyme) we have extended the analysis to the whole protein, finding reproducibly higher (from two independent data sets) average anisotropic motional amplitudes in loop regions ($\sigma_{av} \approx 20°$) than in secondary structure. The importance of incorporating anisotropic motions into RDC analysis for the precise determination of the alignment tensor is particularly evident in this case, where similar values for A_a and A_r are only extracted from the loop and secondary structural elements when GAF-like motions are allowed.

We have also examined the sensitivity of other backbone RDCs present in the peptide plane to anisotropic motion of this kind, and identified the $^{\alpha}C-C'$ vector as the least affected commonly measured ^{1}D coupling. We have therefore used this RDC, in combination with the $N-^{N}H$ RDC, to develop a combined description of GAF-like motions for both RDCs. This simultaneous fitting leads to similar values of motional amplitudes compared to those extracted from $N-^{N}H$ RDC, and, importantly, a more significant improvement with respect to the static model than that extracted using only the dynamically averaged $N-^{N}H$ coupling. One additional advantage of this combined analysis is the increased effective angular sampling available from the additional vector, which allowed us to extract similar average motional amplitudes from four of the five recently published data sets measured from protein G.

Any analytical treatment requiring knowledge of local structure will be susceptible to potential artifacts due to local imprecision in the three-dimensional coordinates, or structural noise. For this reason, we have systematically studied the potential of mistakenly interpreting this noise as dynamics at each step of our analysis. We find that randomly distributed structural noise cannot give rise to the observed anisotropic motional amplitudes detected in the experimental systems presented here. We are also able to demonstrate the sensitivity of this technique to a combination of structural noise and low levels of angular sampling, for example from smaller data sets.

We have further addressed this issue by taking one data set from lysozyme, and fitted this to 13 different resolution crystal structures. There is no evidence that low-resolution structures can be expected to give rise to artificial motions in this resolution range. Analysis using structures from throughout this range reproduces the data with almost equivalently high accuracy, and shows similarly high significance of the dynamic model over the static model. The spread of motional amplitudes from the structures that give a significant improvement over the static model is quite small, suggesting that the method is in fact quite robust with respect to diffraction resolution levels up to 2.1 Å, while the only two structures that do not give statistically significant improvement have very different resolution.

Two advantages of using the GAF-model to describe conformationally averaged RDC can be identified here: the first is that a more accurate definition of the alignment tensor amplitude can be derived using this description. Second, this method allows the detection of average small amplitude anisotropic motions in proteins from relatively easily measurable data, on time scales where motions are not always accessible from other NMR techniques. This information is averaged over data sets containing many RDCs, and therefore only gives an overall picture of average peptide backbone reorientations within these regions. The observation that average motional amplitudes found in secondary structural elements are comparable to the motional amplitudes commonly derived from spin relaxation certainly does not exclude the possibility of significant local fluctuations from this average behavior.

In conclusion, this general approach, of including a known geometric model into the definition of motionally averaged RDCs, will hopefully allow more precise interpretation of RDC for structural and dynamic analysis of proteins in solution.

Acknowledgment. This work was supported by the Commisariat à l'Energie Atomique (France), the Centre Nationale de Recherche Scientifique (France). P.B. is grateful to the European Molecular Biology Organization for a Postdoctoral fellowship. We thank diverse authors for making the RDC data available and the reviewers for generous advice.

Supporting Information Available: Figures showing static and dynamic fits of simulated 1D and 3D GAF data, figures showing angular sampling from two data sets from ubiquitin, and tables showing the rhombicity and Euler angles for the analysis in Tables 1, 3, and 4. This material is available free of charge via the Internet at http://pubs.acs.org.

JA036977W